

Parameterizing Complex Reactive Force Fields Using Multiple Objective Evolutionary Strategies (MOES): Part 2: Transferability of ReaxFF Models to C–H–N–O Energetic Materials

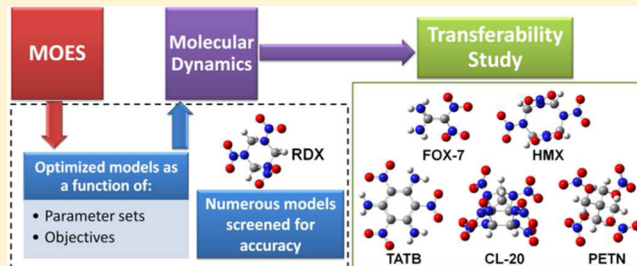
Betsy M. Rice,[†] James P. Larentzos,[‡] Edward F. C. Byrd,[†] and N. Scott Weingarten^{*,†}

[†]Energetic Materials Science Branch, Weapons and Materials Research Directorate, U.S. Army Research Laboratory, Aberdeen Proving Ground, Maryland 21005, United States

[‡]Engility Corporation, High Technology Services Group, U.S. Army Research Laboratory, Aberdeen Proving Ground, Maryland 21005, United States

S Supporting Information

ABSTRACT: The Multiple Objective Evolutionary Strategies (MOES) algorithm was used to parametrize force fields having the form of the reactive models ReaxFF (van Duin, A. C. T.; Dasgupta, S.; Lorant, F.; Goddard, W. A. *J. Phys. Chem. A* **2001**, *105*, 9396) and ReaxFF-lg (Liu, L.; Liu, Y.; Zybin, S. V.; Sun, H.; Goddard, W. A. *J. Phys. Chem. A* **2011**, *115*, 11016) in an attempt to produce equal or superior ambient state crystallographic structural results for cyclotrimethylene trinitramine (RDX). Promising candidates were then subjected to molecular dynamics simulations of five other well-known conventional energetic materials to assess the degree of transferability of the models. Two models generated through the MOES search were shown to have performance better than or as good as ReaxFF-lg in describing the six energetic systems modeled. This study shows that MOES is an effective and efficient method to develop complex force fields.



1. INTRODUCTION

The powerful classical molecular dynamics (MD) method is routinely used to provide atomistic-level descriptions of properties and behavior of materials that span all chemical classes. However, the accuracy and utility of the method has a strong dependence on the description of the interatomic forces used to depict the material and its response under specified conditions. Energetic materials represent an extremely difficult class of materials to model using MD, due to the complexity of the interatomic interactions as well as the need to model chemical reactions that result from subjection to extreme conditions, such as shock and thermal loading. For such systems, reactive force fields are required to depict the proper response of an energetic material to such stimuli while also being able to predict physical-chemical properties of the material at less-extreme conditions.

ReaxFF¹ is currently the only general reactive force field that has been parametrized to describe reactive chemistry of energetic materials and has been applied to C–H–N–O energetic systems including cyclotrimethylene trinitramine (RDX),² pentaerythritol tetranitrate³ (PETN), 1,3,5,7-tetranitro-1,3,5,7-tetraazacyclooctane (HMX),⁴ triamino-trinitrobenzene (TATB)⁴ nitromethane (NM),⁵ and triacetonetriperoxide (TATP).⁶ ReaxFF was designed to be a transferable force field for use in molecular simulations of chemically reacting systems and is parametrized using only quantum mechanical (QM) information. The ReaxFF energy of a system is given as the sum of partial energies

$$\begin{aligned} E_{\text{Reax}} = & E_{\text{bond}} + E_{\text{lp}} + E_{\text{over}} + E_{\text{under}} + E_{\text{val}} + E_{\text{pen}} + E_{\text{coa}} \\ & + E_{C_2} + E_{\text{tors}} + E_{\text{conj}} + E_{\text{Hbond}} + E_{\text{vdW}} + E_{\text{Coul}} \end{aligned} \quad (1)$$

where the partial energy terms are, respectively: bond energy, lone pair energy, corrections for atom overcoordination and undercoordination, valence angle energy (including a penalty function E_{pen}), angle conjugation energy, C_2 correction energy, torsion angle energy, torsion conjugation energy, hydrogen bond energy, van der Waals energy, and Coulomb energy. The atomic partial charges associated with the Coulomb energy are calculated using the Electron Equilibration Method (EEM).⁷

However, as noted by its developers in the development of a modified version of the original ReaxFF force field⁸ (denoted ReaxFF-lg), the DFT information used to parametrize ReaxFF did not properly account for the London dispersion. Therefore, simulations to obtain simple ambient state structural properties of crystals of energetic materials (whose dominant interactions are van der Waals) using ReaxFF produced densities that were unacceptably small. To counter this undesirable feature, ReaxFF-lg was developed to provide correction to dispersion interactions for such molecular crystals, and this function is given as

$$E_{\text{Reax-lg}} = E_{\text{Reax}} + E_{\text{lg}} \quad (2)$$

Received: August 28, 2014

Published: January 20, 2015



where the long-range dispersion correction terms [right-most term in eq 2] are expressed as

$$E_{lg} = - \sum_{ij, i < j}^N \frac{C_{lg,ij}}{r_{ij}^6 + dR_{ej}^6} \quad (3)$$

In eq 3, r_{ij} is the separation distance between atoms i and j , R_{ej} is the equilibrium van der Waals distance between atoms i and j , d is a scaling factor that is set to 1.0, and $C_{lg,ij}$ is the dispersion energy correction parameter. Ambient state crystal densities predicted with ReaxFF-*lg* are in better agreement with experimental values for RDX and PETN (decreasing from -28.45% and -16.88% , respectively, to less than 1% for both cases).⁸ Application of ReaxFF-*lg* to TATB and NM also demonstrated a modest improvement in density predictions for TATB (4.09% error versus -6.30% using ReaxFF) and NM (-6.69% error versus -8.04% using ReaxFF).⁸

In an accompanying paper,⁹ we described the use of the Multiple Objective Evolutionary Strategies (MOES) method to obtain a set of parameters for the original ReaxFF function [eq 1] that would better describe the ambient state crystal structure of RDX. In that study, the 46 parameters corresponding to the van der Waals and EEM were allowed to vary in the MOES search. Also, as reported in that study, we augmented the original training set to include QM energies [calculated using symmetry-adapted perturbation theory based on the Kohn–Sham density functional description, SAPT(DFT)¹⁰] for 1148 RDX¹¹ and 938 1,1-diamino-2,2-dinitroethylene (FOX-7)¹² dimer configurations. SAPT(DFT) results have been shown to be very accurate in modeling dispersion energies. The FOX-7 system is a layered structure, much like TATB, with strong-hydrogen bonding between neighboring molecules within the layers. We hypothesized that inclusion of these more accurate energies in the training set might lead to better descriptions of dispersion forces for the van der Waals terms within the original ReaxFF. In fact, it was noted by the developers that “since no data were included to train these vdW terms to fit the long-range London dispersion, they rather play a role in modulating the various valence interactions by including the Pauli repulsion or steric interactions so important for valence structure.”⁸

In the accompanying study,⁹ the QM information within the original ReaxFF training set and the additional SAPT(DFT) information were used to define five objectives for use in the evolutionary fitting scheme, with the MOES search producing a Pareto-optimal set of force fields. From these, we selected the one that best described the crystal parameters of RDX. No other criterion was considered in this selection. While the results shown in our accompanying paper demonstrate that better crystallographic parameters were generated using the ReaxFF-MOES force field,⁹ subsequent explorations into the limits of the force field revealed that the structures of the molecules within the unit cell were more poorly described than the original ReaxFF force field. This indicates that inclusion of the additional SAPT(DFT) information in the training set led to a set of parameters for the van der Waals terms that improved the weak intermolecular interactions, and thus the overall crystal structure, at the expense of the quality of the valence structures.

In light of these findings, we continue this assessment of using MOES to develop ReaxFF-*lg* force fields, exploring the dependence of results on the number and types of parameters to be determined using MOES, and assessing the ability of the resulting Pareto-optimal force fields to predict various well-known energetic molecular crystals at the ambient state,

including RDX, FOX-7, HMX, 2,4,6,8,10,12-hexanitro-2,4,6,8,10,12-hexaazaisowurtzitane (CL-20), PETN, and TATB. We also explore the sensitivity of the results when separating the SAPT(DFT) information into two groups for separate objective evaluations, where the SAPT(DFT) information for the RDX and FOX-7 dimers reside in separate objectives rather than just one, and compare the force fields to the results obtained in the accompanying study.⁹

The paper is structured as follows: Section 2 provides details of the computational approach, including description of the training set, the parameters that are allowed to vary, the screening procedure used to select the “best” force field from among the Pareto-optimal solutions, and a description of the methods to analyze the crystallographic and molecular structural parameters obtained in molecular dynamics simulations using the force fields. Section 3 describes the application of the force fields to the aforementioned set of energetic crystals to determine transferability. The final section provides a summary of the results and conclusions.

2. COMPUTATIONAL APPROACH

2.1. Overview. The MOES process to generate new parameters for ReaxFF-*lg* is initiated by providing an initial parametrization of the potential function. The ReaxFF-*lg* form is the same as the original ReaxFF force field except for the addition of a term entitled “ E_{lg} ”, a long-range-correction term using the low-gradient model. The initial parameters used in the MOES process are those given in ref 8. The MOES search process starts by first modifying the initial parametrization according to a set of strategy parameters and creates the first generation of parent and child parametrizations. ReaxFF-*lg* models using these parametrizations are used to calculate the energetic and structural properties of numerous chemical structures in our training set. These are then compared with the reference data contained within the training set, which is partitioned into groups, from which “objectives” (i.e., sums of errors for quantities in the group) are evaluated. A new generation of parameters is then created according to fitness functions based on the computed objective errors. This process of creating parametrizations and determining objective errors is repeated until converged parameter sets that cover the Pareto frontiers are obtained. A more detailed description of using the MOES process to generate the ReaxFF parameter sets is given in ref 13 and in the accompanying paper.⁹

A Pareto-efficient parameter set, however, does not imply that it is adequate for use in atomistic simulations. A subsequent assessment must be performed to determine its suitability for problems of interest. In this study, we are interested in determining a force field’s ability to predict the ambient state crystal structure (both crystallographic and molecular structural parameters) of conventional C–H–N–O energetic molecular crystals in MD simulations. Thus, MD simulations using ReaxFF-*lg* and the Pareto-efficient parameters are performed to determine their suitability for predicting these properties of interest. For the purposes of this study, our selections of the “best” force fields are based on those criteria using a screening process in which predicted structures using Pareto-efficient force fields are compared with experimental values.

2.2. Description of Training Set. The original training set for ReaxFF¹ was augmented with highly accurate quantum mechanical information on two C–H–N–O explosives; specifically, single-point energy calculations for 1148 RDX dimer configurations¹¹ and 938 FOX-7 dimer configurations¹²

using the SAPT (DFT)¹⁰ description. The training set consists of nearly 3600 reference data points composed of energies and structures obtained via quantum mechanical calculations. Associated with each reference data point is a corresponding weight. Similar reference data points are grouped together (e.g., energies in one group, geometrical data in another group) from which the corresponding objective function (i.e., error) is calculated

$$\text{Obj}(j) = \sum_{i=1}^{N_{\text{Data}}(j)} \left(\frac{\text{calc}(i) - \text{ref}(i)}{\text{weight}(i)} \right)^2 \quad (4)$$

where j denotes the objective. As discussed in the accompanying paper,⁹ objectives are not assigned weights a priori. From this, the measure of the fitness of each force field from a MOES search is determined. For this study, MOES calculations to search for ReaxFF parameters were performed using five or six objectives, whose compositions are described in Table 1. All information used in the training set is that found in the Supporting Information in the accompanying paper.⁹

Table 1. Description of the Objectives Used in the MOES Search Procedure

index	objective name	composition
Five-Objectives, Type 1		
1	charges	atomic partial charges of various structures
2	geometry	bond lengths, angles and torsions of various structures
3	heat of formation	formation enthalpies of various chemical species
4	frequencies	vibrational Frequencies of various chemical species
5	energy	reaction pathway and bond dissociation energies of chemical species augmented with SAPT(DFT) energies of RDX dimers ¹¹
Five-Objectives, Type 2		
1	charges	atomic partial charges of various structures
2	geometry	bond lengths, angles and torsions of various structures
3	heat of formation	formation enthalpies of various chemical species
4	energy	reaction pathway and bond dissociation energies of chemical species
5	energy	SAPT(DFT) energies of RDX ¹¹ and FOX-7 ¹² dimers
Six-Objectives		
1	charges	atomic partial charges of various structures
2	geometry	bond lengths, angles and torsions of various structures
3	heat of formation	formation enthalpies of various chemical species
4	energy	reaction pathway and bond dissociation energies of chemical species
5	energy	SAPT(DFT) energies of RDX dimers ¹¹
6	energy	SAPT(DFT) energies of FOX-7 dimers ¹²

The difference between the five-objectives, Type 2, and six-objective training sets (Table 1) is in the partitioning of the SAPT(DFT)^{11,12} information. The six objectives training set was explored to determine if partitioning the SAPT(DFT) FOX-7 data from the RDX data would result in a ReaxFF-*lg* type force field that better describes hydrogen bonded systems, such as FOX-7 or TATB.

2.3. Descriptions of Parameters Varied during the MOES Search. In the accompanying study,⁹ parameters within a small subset of the ReaxFF parameters used in ref 6 [the 46 parameters corresponding to the vdW energy and the EEM in eq 1] were optimized using the MOES search process and five

objectives, Type 2. The parameter set that best predicted the crystal structure of RDX produced results that were in significantly better agreement with experimental crystal parameters than those produced using the ReaxFF parameters in ref 6, but at the expense of the description of the molecular structures, as will be shown hereafter. Attempts at MOES parametrizations on ReaxFF parameter sets in which 500 parameters were allowed to vary did not yield converged results using supercomputing resources available to us. In order to obtain adequate coverage of the Pareto frontier, we have found that using an evolving population roughly an order of magnitude larger than the number of parameters to be optimized usually leads to reasonable convergence.⁹ This effectively limits a MOES optimization to approximately 100 parameters using the current generation of high performance computing platforms. Subsequently, we restricted our MOES parametrizations to small subsets of ReaxFF-*lg* parameters; these include the 8 parameters that correspond to the long-range-correction terms, the 46 parameters that correspond to the vdW energy and the EEM, the 54 parameters corresponding to the sum of these parameter sets, or the 62 parameters corresponding to the vdW, EEM, long-range-correction and H-bond terms. As described in the accompanying paper,⁹ the calculations averaged 50K CPU hours on an average of 200 cores per evolution. ReaxFF-*lg* force fields resulting from MOES searches for each combination of parameter set size and number of objectives are denoted by the model identifier given in Table 2.

2.4. Screening the Pareto Efficient Parameter sets with Molecular Dynamics for RDX. The RDX ambient state crystal structural information was used to assess the quality of the MOES-generated Pareto-efficient solutions determined in this paper (i.e., the ReaxFF and ReaxFF-*lg* parameter sets). This assessment was obtained from results of a series of MD screening calculations using each of the Pareto-efficient parameter sets (which can number in the hundreds as shown in Table 2) for RDX for each of the eight models tested. All calculations were performed using the LAMMPS simulation software.¹⁴ The screening was conducted in two phases. For the first screening phase, a series of MD simulations in a variety of ensembles was performed to relax the system away from the initial configuration in the simulation cell. Details of the simulation cells for RDX (and all other systems studied herein) are given in Table 3; the initial crystallographic and molecular parameters correspond to the experimental geometry. Figure 1 shows the molecular structures of the compounds modeled in this study.

As the first step in the initial phase of screening, a short microcanonical (NVE) simulation is initiated to relax the system away from the initial configuration; atomic velocities are scaled at each step to drive the system to $T = 300$ K. The NVE simulation is followed by a short isothermal–isochoric (NVT) MD simulation at 300 K to equilibrate the temperature, followed by a longer simulation within the isothermal–isobaric (NPT) ensemble, during which the lengths of the cell edges are allowed to change independently (the cell angles are fixed). At the end of the NPT simulation during this first phase of screening, the lattice constants are compared to the experimental values for RDX, and a subset of force fields that have arbitrarily defined “acceptable” errors in unit cell volume and edge lengths are selected for the second phase of screening simulations. The arbitrarily defined acceptable degrees of error in calculations using the various models are given in Table 2, (degrees of error were chosen to select approximately ten force fields); no other structural information was used to determine suitability for the

Table 2. Description of the MOES ReaxFF Models

model	formalism	objective name	No. of params. varied	description of varied params.	No. of Pareto efficient solutions	No. of Pareto efficient solutions satisfying edge length error criteria
1	ReaxFF [eq 1]	5 objectives, Type 1	46	vdW, EEM	604	8 satisfy a 0.5 Å edge length error criterion
2	ReaxFF [eq 1]	5 objectives, Type 2	46	vdW, EEM	556	8 satisfy a 0.5 Å edge length error criterion
3	ReaxFF-lg [eq 2]	5 objectives, Type 2	8	long-range correction	880	15 satisfy a 0.38 Å edge length error criterion
4	ReaxFF-lg [eq 2]	5 objectives, Type 2	46	vdW, EEM	705	10 satisfy a 0.22 Å edge length error criterion
5	ReaxFF-lg [eq 2]	5 objectives, Type 2	54	vdW, EEM, long-range correction	576	11 satisfy a 0.22 Å edge length error criterion
6	ReaxFF-lg [eq 2]	6 objectives	8	long-range correction	1759	13 satisfy a 0.32 Å edge length error criterion
7	ReaxFF-lg [eq 2]	6 objectives	54	vdW, EEM, long-range correction	1007	9 satisfy a 0.2 Å edge length error criteria
8	ReaxFF-lg [eq 2]	6 objectives	62	vdW, EEM, long-range correction, hydrogen bond	816	12 satisfy a 0.25 Å edge length error criterion

Table 3. Description of Simulation Boxes for Energetic Molecules Crystals

name	CSD reference code ¹⁵	space group	No. of molecules in unit cell	composition of supercell	ref. for experimental crystal structure
RDX	CTMTNA	Pbca	8	2 × 3 × 3	16
HMX	OCHTET12	P2 ₁ /c	2	5 × 3 × 4	17
CL-20	PUBMUU02	P2 ₁ /n	4	4 × 3 × 3	18
PETN	PERYTN12	P̄421c	2	3 × 3 × 3	19
FOX-7	SEDTUQ01	P2 ₁ /n	4	4 × 4 × 3	20
TATB	TATNBZ	P̄I	2	3 × 4 × 5	21

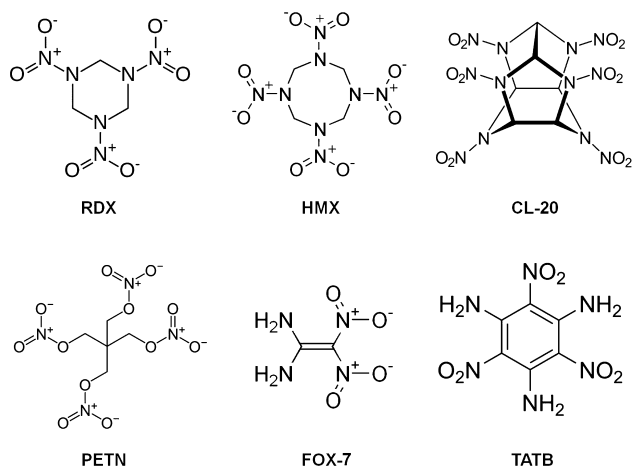


Figure 1. Illustration of the six molecules for which ambient-state crystal structures were predicted using various models based on the ReaxFF and ReaxFF-lg formulas [eqs 1–3].

second phase of screening simulations. The number of Pareto-efficient solutions that satisfied the arbitrarily defined criteria for the RDX system is given in Table 2.

In the second phase of screening, isothermal-isostress (NsT) MD simulations at room temperature and pressure for RDX were performed, using as initial conditions the atomic positions and velocities at the end of the NPT simulation performed during the first phase of screening. Crystallographic parameters averaged over the “production” interval of this simulation (i.e., the last 10 ps) were compared with experiment and used to identify the best-performing force fields within each of the ReaxFF models described in Table 2. Time step sizes for all simulations in this study are 0.25 fs; the NVE and NVT portions of the screening simulations were each integrated for 2.5 ps (10 000 steps), while the NPT and NsT simulations were integrated for 7.5 ps (30 000

steps) and 25 ps (100 000 steps), respectively. The damping parameters for the thermostat and barostat are 0.05 and 0.5 ps, respectively.

Transferability of the best-performing models to the other energetic molecular crystals listed in Table 3^{15–21} was explored by performing a series of MD simulations for each system that are similar to those performed for RDX during the screening and production phases described above (i.e., NVE, NVT, NPT, and NsT simulations).

Atomic configurations and lattice vectors were recorded at 500 time-step intervals (0.125 ps) during the NsT simulations; the last 80 snapshots corresponding to the final 10 ps of each trajectory were used to calculate the time-averaged crystallographic and molecular structural properties, as described in the next section.

2.5. Crystallographic and Structural Analysis. Quantities that are compared against experiment are time-averaged crystallographic parameters and time- and spatially averaged molecular structural parameters [fractional positions of the mass centers (s_x , s_y , and s_z) and orientation of each molecule in the unit cell as well as the internal atomic structure of each molecule]. The molecular structural parameters for each symmetry-equivalent molecule in the unit cell were averaged over all unit cells that make up the supercell. We did not use Euler angles to describe the orientation of the molecules in the unit cell, as these are determined using a rotation matrix that transforms the body-fixed molecular frame (which is typically the principal axes of inertia) to the space-fixed coordinate system. Comparison of predicted and experimental Euler angles would be appropriate only if the predicted and experimental molecular structures were the same (or very similar). Because some of the models reported here generated molecular structures that differed significantly from the experimental structures, Euler angles derived from the resulting body-fixed frame would reflect deviations from experiment due to both structural deformations and molecular

orientation. Thus, an alternative approach was used to determine the deviation from experiment of the molecular orientation of each symmetry equivalent molecule in the unit cell.

This alternate approach involves first determining the overall deviation (due both to structural deformation and orientation in the unit cell) from experiment, and subtracting out the differences due to molecular deformation. To determine the overall deviation of each symmetry equivalent molecule from experiment, the mass centers of the experimental and time- and spatially averaged predicted molecules were superimposed, and the root-mean-square (rms) deviation of the atomic displacements of the predicted structure from the experimental counterpart was evaluated. This value encompasses deviations of the predicted structure from experiment, due to both molecular orientation and structure.

Next, the deviation of the predicted structure from the experiment due solely to molecular structural differences is determined using the method proposed by Kearsley,²² which involves obtaining the rotational matrix that minimizes the sum of the squared distances between corresponding atoms in the two structures being compared and then using it to produce an optimal superposition of the calculated structure onto the experimental counterpart. Rms deviations of predicted atomic displacements of the rotated predicted structure from the experimental structure are evaluated. An estimate of the deviation from experiment due to the orientation of the molecule in the unit cell is given as the difference between the total and structural rms.

These quantities, along with the predicted and experimental crystal parameters and densities, are given in Tables S1–S6 (see Supporting Information) for each crystal considered in this study. The absolute maximum deviation of the predicted atomic displacements from the experimental positions for each of the symmetry-equivalent moieties due to structural or orientational differences is also given. Furthermore, Tables S1–S6 contain averaged center-of-mass fractional positions of each symmetry-equivalent moiety, derived from cumulative distributions of these quantities obtained during the trajectory integrations, along with the corresponding absolute error from experiment. For ease in evaluation of molecular structural information in the case of the PETN crystals, the positional and orientational information are given for each asymmetric moiety within the unit cell, which corresponds to one-fourth of a PETN molecule.

3. RESULTS AND DISCUSSION

3.1. RDX Crystal. The quality of ReaxFF force fields using parameters generated from a MOES search as described above was assessed in the prediction of the ambient state crystal structure of RDX. In addition to comparing these results with experimental values, the results were compared to those produced in NsT-MD simulations using the original ReaxFF⁶ and ReaxFF-*lg*⁸ parameters, respectively. With the exception of the original ReaxFF force field,⁶ all other models (including ReaxFF-*lg*) differ from the experimental density by no more than 1.1%. However, in most of the results, there is a cancellation of errors in the individual cell edge lengths that result in the equally good agreement in density demonstrated by the models. For example, the percent errors for lattice parameters *b* and *c* for the ReaxFF-*lg* model are –3.6 and 2.6%, respectively; Models 3 and 6 show similar offsets. Model 5 has the closest agreement with experiment in density and best overall agreement with experiment in all edge lengths. All models roughly maintain the orthorhombic cell structure, with most having deviations of

the cell angles from experiment of no more than 0.4°. The exceptions are Models 2, 7, and 8, having deviations up to 1.3°, 1.1°, and 1.5°, respectively.

Predicted crystallographic and molecular structural information for the contents of the RDX unit cell predicted using all models is compared with experimental information in Supporting Information Table S1. This information is given for each molecule in the unit cell, with fractional positions of the molecular mass centers and molecular structure averaged over all unit cells within the supercell over the last 10 ps of each trajectory. Table S1 also provides the error in these parameters averaged over all molecules in the unit cell.

Models 1 and 2 have the worst overall performance in locations of the molecular mass centers within the unit cell, with the largest being in the direction along the *b* axis of the unit cell. The best overall performance is shared by Models 3 and 5. With regard to deviation of molecular structures, Model 1 had the largest average rms deviation from experimental values (0.552 Å). With regard to lattice parameters, Models 1 and 2 both showed significant improvements over the original ReaxFF model using eq 1 only (i.e., no *lg* terms), but clearly, the molecular structure was affected by the changes in parameters required to get the better agreement with lattice parameters. Likewise, modification of the hydrogen bonding terms (i.e., Model 8) influenced molecular structural changes. Similarly, the rms deviation from experiment of the orientations of the molecule for Model 1 was also the largest among all force fields. Models 7, 8, and 4 produced the smallest rms deviations from experiment of the orientations of the molecule. Models 7 and 4 also have the best performance for molecular structure; however, some structural differences are significant. For example, the equatorial N–N bond in Model 7 is 1.51 Å compared to that of the experimental structure (1.35 Å). Similarly for the same Model, the axial N–N bonds are 1.49 and 1.52 Å whereas the experimental values are ~1.4 Å. Figure 2 shows the optimal superposition for the models that predict the best and worst performances (Models 7 and 1, respectively) for the molecular structure of RDX. The largest deviation from experiment for Model 7 appears localized in the region of the equatorial N-NO₂; the predicted ring structure is flatter than that of experiment. Conversely, the predicted deviation from molecular structure for Model 2 does not appear localized to a single region but poorly predicts both ring and alignment of CH₂ and N-NO₂ moieties.

As we have seen, no one model is optimal to describe all aspects of RDX. In an attempt to encapsulate and quantify the multitude of various structural data metrics used to evaluate the performance of a model, we used a simple ranking procedure. A measure of the overall quality of each force field is obtained through the rankings of each force field according to its errors in predictions of the various crystallographic and molecular structural parameters, as given in Table 4. Higher ranks (e.g., a rank of 1 or 2) are assigned to models with lower errors. The overall ranking for the force field is simply the sum of the rankings for the individual categories, with the force field having the lowest value designated as the “best”. Models that receive the same rank are assigned an average rank value (e.g., two models tied for third would each receive a rank of 3.5 [average of third and fourth]). This method for identifying the most suitable force field is approximate and is dependent on the definition of the categories used to determine quality. For our purposes, we are interested in the ability of the force field to predict crystallographic structures at the ambient state. For RDX, Models 4 and 5 have the best overall performances according to this measure.

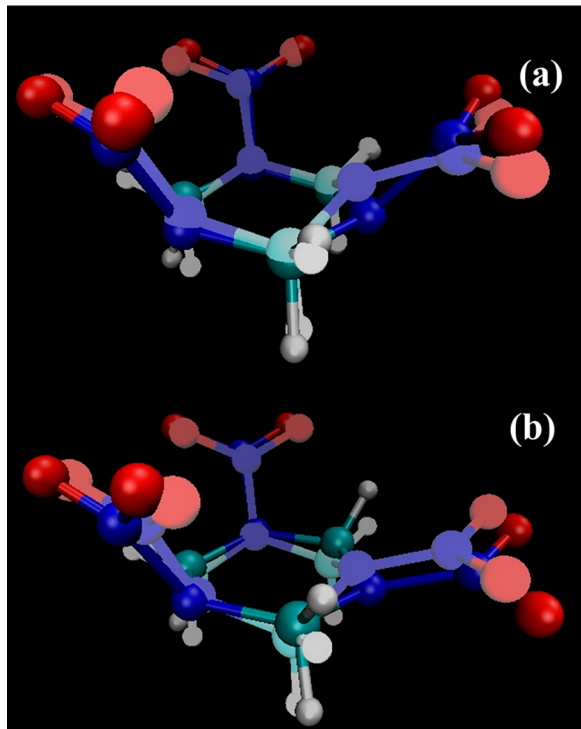


Figure 2. Pictorial views of the time and spatially averaged molecular structure for one of the symmetry equivalent molecules in the RDX crystal superimposed onto the experimental structure (translucent) at the ambient state for (a) Model 7 and (b) Model 1.

As the design concept behind ReaxFF is for the force field to be as general as possible, it is useful to determine the transferability of these force fields to other energetic molecular crystals, since each was selected because of its ability to best describe RDX. We note that information about HMX, TATB, PETN, and FOX-7 was used in the training sets for all models (both by the original developers and by ourselves) with one exception: FOX-7 information was not used in the training sets for parametrizing the original ReaxFF, ReaxFF-*lg*, and Model 1. However, the combined number of data points for HMX, TATB, and PETN are approximately two orders of magnitude less than those used for RDX and FOX-7. This information is given in the Supporting Information to the accompanying paper.⁹ Thus, the HMX, TATB, and PETN information might impose some influence on the transferability of the models in describing these systems. However, the models for which transferability will be explored

were selected in the preliminary screening as best representing the ambient-state RDX crystal.

3.2. HMX Crystal. As for the RDX system, the density predicted by the original ReaxFF force field is in significantly larger disagreement than for other models except Model 2, which is only slightly smaller (Supporting Information Table S2). However, Model 2 exhibits an extremely large error in all three edge lengths (-19.8% , 18.3% , and -20.3%), and it is only a cancellation of errors in these edge lengths that results in a density error that is lower than that of ReaxFF. Also, the reasonable agreement in density for Model 1 is due to a cancellation of unacceptably large errors in two of the cell edge lengths (-14.9 and 11.9% errors in the b and c edges, respectively). Only Models 3 and 6 and ReaxFF-*lg* have errors in cell edge lengths and densities that are less than 3%. The HMX crystal is a monoclinic system, having two angles that are 90° , and one non- 90° angle, in this case, the β angle. All force fields predicted the α angles to be within 0.2° of the experimental value. The error in the predicted β angle was the largest for Model 2 (-23°) while Models 4, 5, and 7 predicted this angle to within 0.5° of the experimental value. As evident in Table S2, all of the models had very small errors with regard to the location of the fractional molecular mass centers within the unit cell. The average rms deviations from experiment of the molecular structures for all but four models (ReaxFF and Models 1, 2, and 8) were approximately 0.2 \AA . The average rms orientational structural deviations for all but one of the models were less (in some cases significantly) for the HMX system when compared to those of RDX. For example, the average rms orientational deviations for HMX predicted using ReaxFF-*lg* and Model 6 are respectively 0.075 and 0.071 \AA , compared to 0.604 and 0.631 \AA for the RDX case.

The rankings by category and overall rankings of the models are given in Table S5; three models have an approximately equivalent overall rank: ReaxFF-*lg* and Models 5 and 6, with ReaxFF-*lg* having a slightly lower score. Models 2, 8, and ReaxFF were the poorest overall performers.

3.3. CL-20 Crystal. Similar to the RDX and HMX systems, the original ReaxFF poorly describes the cell edge lengths and density of the CL-20 system (Table S3). Unlike those systems, however, the errors in the predicted densities and cell edge lengths for many of the models exceed 3%; only Models 1, 2, 4, and 7 have densities within 3% of the experimental value, but offsets in the errors for the cell lengths and error in the β angle produce this apparent good agreement. Also, unlike the HMX system, the error in the edge lengths predicted by Model 2 are much less than those predicted by ReaxFF, although the error in

Table 4. Ranks of Models by Lowest Error for RDX

model	edge lengths ^a	cell angles ^b	COM fractionals ^b	molecular structure ^c	orientation ^c	overall rank
1	6	4	9	10	10	39
2	4	9	10	8	9	40
3	9	7	2	7	8	33
4	2	3	5	2	3	15
5	1	1	1	3	4	10
6	8	5	3	6	7	29
7	5	8	8	1	1	23
8	3	10	6	9	2	30
ReaxFF	10	6	7	4	5	32
ReaxFF- <i>lg</i>	7	2	4	5	6	24

^aAverage absolute percent errors. ^bAverage absolute errors. ^cAverage rms errors.

Table 5. Ranks of Models by Lowest Error for HMX

model	edge lengths ^a	cell angles ^b	COM fractionals ^b	molecular structure ^c	orientation ^c	overall rank
1	8	4	1.5	8	9	30.5
2	10	10	1.5	9	10	40.5
3	3	7	9	4.5	4	27.5
4	5	3	4	2	7	21.0
5	4	1	6.5	1	5	17.5
6	2	5	4	4.5	2	17.5
7	6	2	8	6	6	28.0
8	9	9	10	10	1	39.0
ReaxFF	7	8	6.5	7	8	36.5
ReaxFF-lg	1	6	4	3	3	17.0

^aAverage absolute percent errors. ^bAverage absolute errors. ^cAverage rms errors.

Table 6. Ranks of Models by Lowest Error for CL-20

model	edge lengths ^a	cell angles ^b	COM fractionals ^b	molecular structure ^c	orientation ^c	overall rank
1	2	1	3	3	3	12
2	6	5	4	7	5	27
3	9	8	9	8	9	43
4	5	4	1	1	4	15
5	7	6	6	4	6	29
6	8	9	7	6	8	38
7	4	3	2	2	2	13
8	3	2	5	10	1	21
ReaxFF	10	7	10	9	10	46
ReaxFF-lg	1	10	8	5	7	31

^aAverage absolute percent errors. ^bAverage absolute errors. ^cAverage rms errors.

Table 7. Ranks of Models by Lowest Error for PETN

model	edge lengths ^a	cell angles ^b	COM fractionals ^b	molecular structure ^c	orientation ^c	overall rank
1	9	4.5	2	7	2	24.5
2	7	9	9	9	9	43.0
3	5	4.5	7	4	6	26.5
4	8	7	3	5	4	27.0
5	4	4.5	4	1	7	20.5
6	3	1	6	2	5	17.0
7	6	8	5	6	1	26.0
8	1	10	10	10	10	41.0
ReaxFF	10	4.5	1	8	3	26.5
ReaxFF-lg	2	2	8	3	8	23.0

^aAverage absolute percent errors. ^bAverage absolute errors. ^cAverage rms errors.

two of the edge lengths is unacceptably large ($\sim 6\text{--}7\%$). No model predicts cell edge lengths that are within 3% of experiment for all directions along the cell axes; ReaxFF-lg has the overall best agreement with experiment for this category. However, ReaxFF-lg, ReaxFF, and Models 3 and 6 underestimate the β angle for this monoclinic system by $\sim 13^\circ$. Model 8 has the closest agreement with the measured value and is within 0.5° of experiment. With regard to the location of the molecular mass centers within the unit cell, Model 4 has the smallest deviation from experiment of all the models. All but Models 1 and 7 have substantially larger overall deviations. Model 4 also has the smallest deviation from experimental molecular structural values. Models 1, 2, 4, 7, and 8 exhibit orientational rms deviations from experiment of $0.2\text{--}0.3\text{ \AA}$; all other models have significantly larger errors. In terms of overall rank (Table 6), Models 1, 4, and 7 share approximately equal low scores, rendering them the “best” performers, with Model 1 having the smallest of the three.

3.4. PETN Crystal. As shown in Supporting Information Table S4, only two models (Models 4 and 8) predict a crystal density within 3% of experiment; however, the good agreement of Model 4 is due to offsets in the errors of individual cell edge lengths. While Model 8 clearly best predicts both density and cell edge lengths, ReaxFF-lg and Models 3, 5, and 6 all have errors in predicted densities of less than 3.9%. For these four force fields, error in the cell edges along the a and b axes are less than 1%, while the error along the c axis ranges from 2.4 to 2.9%. All force fields well predict the cell edge angles to within 0.1° of experiment, with the exception of Model 8 with a deviation of 0.8° degrees in the γ angle. Average absolute errors in the location of the mass centers of the eight asymmetric units of PETN are similar and small for all models but two (Models 2 and 8), with the ReaxFF force field showing the best performance in this category (Supporting Information Table S4). Similarly, with the exception of Model 8, the average rms deviations of molecular structural parameters are almost the same for all

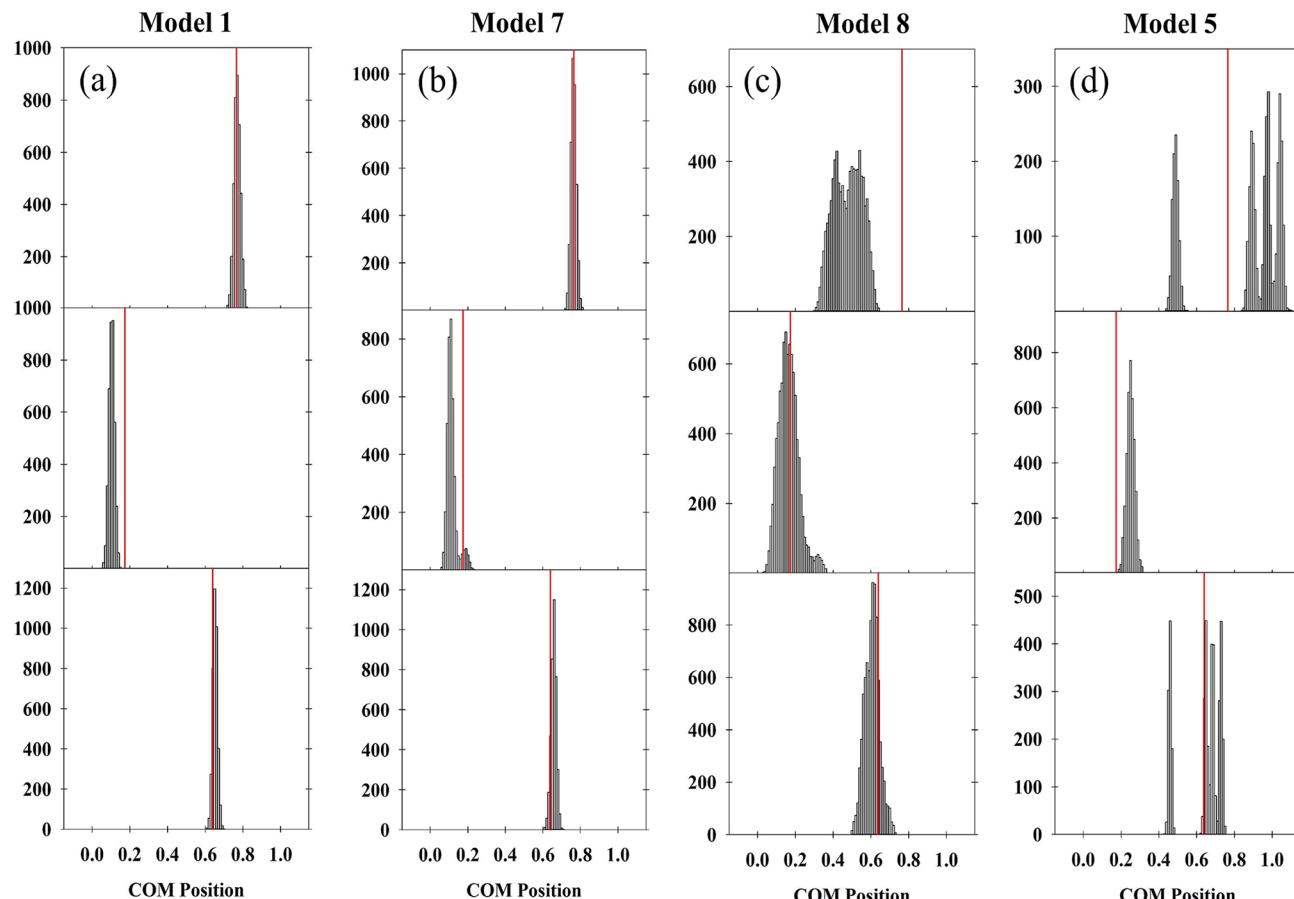


Figure 3. Cumulative distributions of the center-of-mass fractional coordinates for one of the four symmetry equivalent molecules in the unit cell of FOX-7 for (a) Model 1; (b) Model 7; (c) Model 8; (d) Model 5. Top, middle, and lower frames for each model are the distributions for the *x*-, *y*- and *z*-fractional positions, respectively. Red vertical line in each frame denotes the experimental position.

models and are smaller than those for the RDX, HMX, and CL-20 systems. The average rms deviations of orientational structural parameters are small for all models but 2 and 8, and are ~ 0.1 Å. According to the results shown in Table 7, Model 6 has the best overall rank, and Models 2 and 8 were almost equally the overall worst performers

3.5. FOX-7 Crystal. The FOX-7 crystal consists of layers of molecules arranged in a herringbone fashion and has a network of hydrogen bonding within the layers. Therefore, this system exhibits a different type of weak intermolecular interaction than that seen in the previously described molecular crystals. Three of the models predicted crystal densities within 3% of experiment (ReaxFF and Models 1 and 2), with Model 8 only slightly higher (3.2%); however, the good agreement for all models was due to offsets in cell edge lengths and deviations in cell angles (Supporting Information Table S5). All models showed significant deviation in cell edge lengths, with ReaxFF predictions being closest to experimental values. FOX-7 is a monoclinic crystal system, but it is close to orthorhombic, having a β angle of 90.61° . Seven of the models predicted this angle to within 2° of experiment, with Model 2 having the closest agreement (within 0.3°). However, Model 2 had deviations of 1.6 and 1.4° for the other two cell angles; only ReaxFF, ReaxFF-*lg*, and Models 3, 6, 7, and 8 had very small deviations from 90° . Overall, ReaxFF provided the best description of cell edge angles for this system.

Atomic displacements due to deviation of molecular structure are smallest for Model 7, and largest for Models 1 and 8. Surprisingly, Model 8 (the force field resulting from a MOES

search in which the hydrogen-bonding parameters were allowed to vary) produced significantly distorted molecular structures in which intramolecular hydrogen-atom migration appears to occur between the hydrogens on the amine nitrogens and the oxygens from the nitro groups. Six of the models had very similar rms deviations of 0.27 – 0.29 Å in molecular structure (ReaxFF, ReaxFF-*lg*, Models 3, 4, 5, and 6).

Examination of snapshots taken during the trajectory integration revealed that the molecular mass centers of the molecules underwent significant translational motion within the unit cell for all models except Models 1 and 7 during the simulation. The translation is captured in the cumulative distributions of the locations of mass centers in fractional units shown in Figure 3, from which the time and spatial averages were determined from the distributions for four of the models. Figure 3a shows the distributions along each lattice vector for one of the four molecules in the unit cell for Model 1 and represents a case in which the mass centers remain near a lattice site throughout the duration of the last 10 ps of the NsT trajectory. For this model, the sites coincide with the experimental values (denoted with vertical red line in the figure) in the *x*- and *z*-directions, with a slight offset from the experimental position in the *y*-direction. We note that while the molecules are in the correct position within the unit cell, other structural parameters such as lattice vectors and molecular structure are poorly described. Parts b and c of Figure 3 show the distributions for two models in which some of the distributions have a bimodal shape. Average positions taken from such multimodal distributions could be

significantly different from the experimental values. The distributions for Model 7 [Figure 3b] are monomodal in the x - and z -directions; the distribution in the y -direction is bimodal, with a very small mode close to the principal mode. In this case, the small mode in the y -direction does not significantly affect the average value resulting from the overall distributions. The distributions for Model 8 [Figure 3c] shows broad, almost monomodal distributions, indicating that motion of the molecular centers about the lattice sites is large (and in the case of the x -direction, centered about the wrong location). Finally, Figure 3d shows a strong multimodal distribution for locations of the mass center of this molecule as described by Model 5, with the corresponding error reflected in the averaged value.

The orientational deviations of the molecules are all large, with three models predicting deviations from 0.30 to 0.38 Å (Models 7, 8 and 2) and the remaining models predicting rms deviations of 0.55 Å or more. These orientational deviations are clearly apparent in visual comparisons of the predicted atomic arrangements of the four molecules in the unit cells with those in the experimental cell (Figure 4). Model 7 most closely

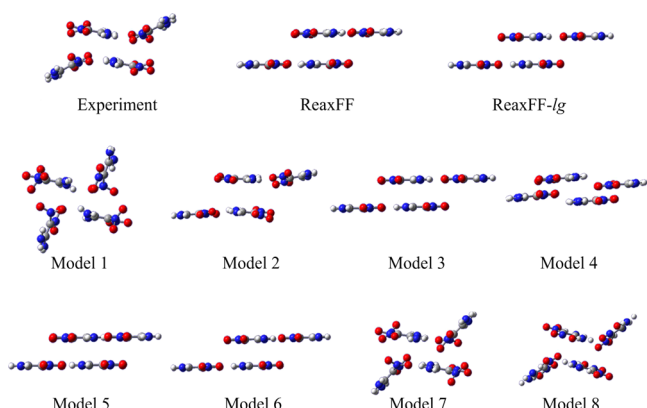


Figure 4. Experimental and predicted FOX-7 unit cells.

resembles the experimental cell, although Models 1 and 8 also show a herringbone structure. However, the herringbone angles in Model 1 are more acute than those of Model 7 when compared to the experimental structure, explaining the higher orientational deviation of this model. The remaining models predict planar graphitic structures, which accounts for the larger deviations from experiment.

Movies of the complete simulation for ReaxFF-lg and Model 7 are included as Supporting Information. Figures 5 and 6 show a series of images from the ReaxFF-lg and Model 7 simulations, respectively. The first image is (a) the initial configuration, followed by snapshots taken at (b) the start of the NsT portion of the simulation, and (c) the final configuration. The three panels show, from left to right, views down the z -, x - and y -axes, with atomic positions projected onto the orthogonal plane. When viewing along the x -axis (middle image) in Figure 5c, we see that the herringbone structure of the FOX-7 crystal is not maintained with the ReaxFF-lg potential. The crystal planes are observed to oscillate between the configurations seen in Figure 5b and c, which explains the large center of mass displacements mentioned above. The herringbone structure remains with Model 7, as seen in Figure 6c, but a defective region exists [circled in Figure 6b] in which some molecules have rotated out of alignment. Note that this region is not visible in the xy - and xz -projections. This occurs

in order to accommodate the shear stress imposed on the crystal prior to the NsT portion of the simulation. The shear stress results in the increase in the β angle to a final averaged value of 95.5°.

The overall rankings show that Model 7 best predicts the FOX-7 crystal because the molecular mass centers do not translate during the trajectory integration, reasonably reproducing the herringbone lattice structure as well as producing the lowest rms deviation in both molecular and orientational structure (Table 8). ReaxFF and Model 4 produced the best cell edge lengths, and both had similar rms deviations in the molecular structure of 0.28 and 0.27 Å, respectively.

3.6. TATB Crystal. Similar to FOX-7, TATB exhibits strong hydrogen bonding. The three models that do not include the long-range correction terms (ReaxFF and Models 1 and 2) predict crystal densities that are within 3% of experiment (see Supporting Information Table S6); however, offsetting errors in the edge lengths and/or cell angles results in the favorable prediction of densities for these models. Predicted cell edge lengths for the a and b dimensions are very close to experimental values using the ReaxFF force field, as opposed to those predicted by Models 1 and 2, but the model produces larger errors for the α and β angles than those given by Model 1. Cell edge lengths for the remaining models are within 1.3% for the a and b dimensions; only ReaxFF-lg and Model 3 produce values for the c dimension that are within ~3% of experiment. With regard to the cell edge angles, all of the models predict the γ angle to within 0.3°, and Models 1, 4, and 5 also predict the β angle to within 0.7° of experiment. Models 1 and 8 are the only models that predict the α angle to within 0.7° of experiment.

As seen for FOX-7, the cumulative distributions of the locations of the molecular mass centers indicate significant translation of the molecules occurs during the trajectories for all but Model 2, but only in the x - and y -directions. As the nearly planar TATB molecules are arranged in graphitic-like layers that are parallel to the $a-b$ plane (i.e., the x - and y -directions in these simulations), the distributions show that the molecules undergo significant in-plane translational motion, while little occurs in the direction perpendicular to these planes. This is reflected in the large error in the averaged locations given in Supporting Information Table S6 along the x - and y -directions, with Figure 7 illustrating typical distributions for those models that produce the averaged values. Clearly, the various models do not adequately capture the extensive in-plane hydrogen bonding of this system that is believed to be the source of its exceptional insensitivity to shock, impact, or heating. Movies of the complete simulation for ReaxFF-lg and Model 7 are included as Supporting Information. Figure 8 shows snapshots for ReaxFF-lg (a–c) and Model 7 (d–f) viewed along the x -axis, with atomic positions projected on to the yz -plane, at the same times as Figures 5 and 6. The shape of the simulation cell changes, and we observe planar motion of the molecular layers. None of the models resulted in the correct stacking of molecular centers among the layers in the z -direction. Furthermore, the molecules in the ReaxFF-lg model remain more planar than in Model 7, where many of the hydrogen bonds form nearly 90° angles with the molecular plane.

Model 5 has the lowest rms molecular structural deviation while Model 2 had the highest. In terms of orientational displacements, all but Model 2 had a relatively small rms orientational displacement (0.06–0.16 Å) compared to those of some of the models for the other systems in this study. Thus, the more significant errors in the description of TATB appear to be in the crystal parameters and the locations of the molecules

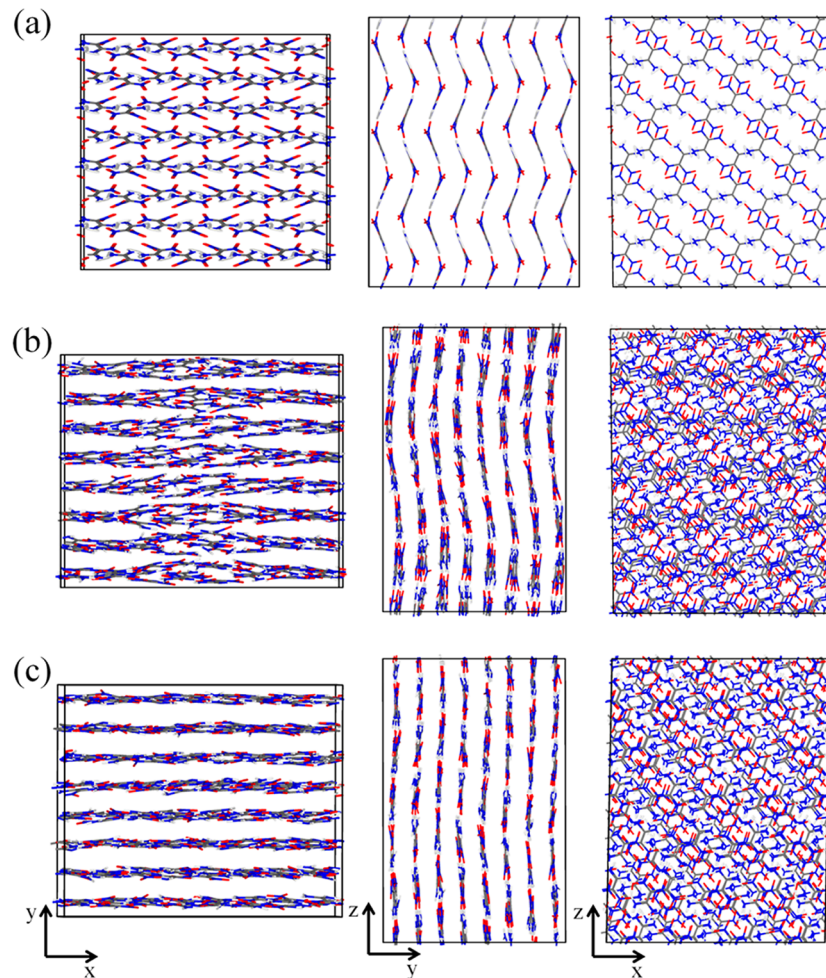


Figure 5. Atomic configurations from a simulation of FOX-7 using the ReaxFF-*lg* potential at (a) the beginning of the simulation (0 ps), (b) at the start of NsT-MD (12.5 ps), and (c) the final configuration (37.5 ps). The images on the left, center, and right are views down the *z*-, *x*-, and *y*-axes, respectively.

within the graphitic-like sheets. Table 9 shows that ReaxFF-*lg* has the best overall rank by far among the models in ability to describe TATB while Model 2 displays the worst performance.

3.7. Comparative Ranking over All Systems. Table 10 compiles the results for all models and molecules and presents an overall rank for each model, displayed in order of best to worst. Model 5 had the lowest overall score (consisting of the ReaxFF-*lg* functional with MOES optimizing the vdW, EEM and *lg* parameters with five objectives), as a result of having ranked within the top three models for four of the systems. Model 7 (same as Model 5 except with six objectives) and ReaxFF-*lg* tied for the next lowest score, followed by Model 4 (same as Model 5 optimizing the vdW and EEM parameters only). Models 8 and 2 were the poorest performers, with Model 2 holding the lowest rank for four systems.

It is important to note that the results of this study are dependent on the force fields that were selected as the most promising from each MOES search according to a user-specified set of criteria. The criteria that were used to select them were subjectively chosen and based solely on the force field's ability to predict the ambient state crystal structural parameters of RDX using molecular dynamics. Had we expanded the selection criteria to include other factors (such as reproduction of reaction pathways), it is likely that different force fields would have been chosen for this study. This subjectivity and associated difficulties

in selection of a single solution from a set of Pareto-optimal solutions is well-known, with more formal research being conducted^{23–27} to cull the most promising candidate solutions. However, the focus of this study is to determine if force fields with the ReaxFF or ReaxFF-*lg* form can be generated using the MOES procedure that will perform as well as or better than the original parametrization toward this user-specified set of criteria, while not requiring user intervention in crafting optimal parameters but rather allowing evolutionary techniques to self-select optimal force fields. Table 10 indicates that it is indeed possible to obtain an optimal ReaxFF-*lg* force field without requiring intense user intervention through application of MOES. However, the parameters allowed to vary in this work did not result in an improvement in predicting crystal structures using the ReaxFF form, supporting the assertion⁸ that a correction to the ReaxFF form was necessary to provide a proper description of dispersion interactions.

We recognize that the ability of ReaxFF and ReaxFF-*lg* to explore complex chemistry using molecular simulation is the primary reason for their popularity. Thus, it is of interest to know the performance of the various models in reproducing the objective entitled “Reaction Pathway and Bond Dissociation Energies” in the original nitramine training set. Figure S1 in the Supporting Information provides a comparison of the performance of the original ReaxFF and ReaxFF-*lg* models and the eight

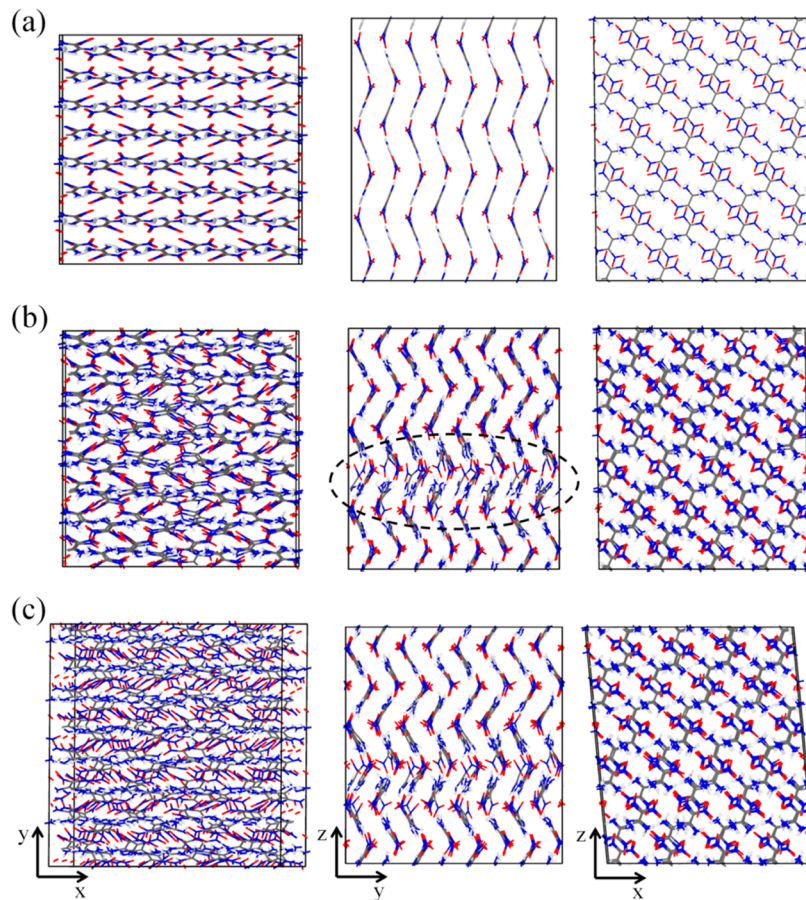


Figure 6. Same as Figure 5, using Model 7. The dashed oval in (b) highlights a defective region of the crystal.

Table 8. Ranks of Models by Lowest Error for FOX-7

model	edge lengths ^a	cell angles ^b	COM fractionals ^b	molecular structure ^c	orientation ^c	overall rank
1	10	9	2	10	10	41
2	8	5	5	8	3	29
3	7	4	4	6	8	29
4	2	7	3	2	4	18
5	9	10	9	4	7	39
6	5	2	6	5	6	24
7	4	6	1	1	1	13
8	3	8	10	9	2	32
ReaxFF	1	1	7	3	5	17
ReaxFF-lg	6	3	8	7	9	33

^aAverage absolute percent errors. ^bAverage absolute errors. ^cAverage rms errors.

MOES models in reproducing the reaction path information in the original nitramine training set. Models 2, 3, and 6 were in equally good agreement with the original ReaxFF and ReaxFF-lg models, all having rms deviations from the reference data of ~71.5 kcal/mol. It is interesting that the worst performer in terms of crystal and molecular structural prediction in this study (Model 2) had the same rms deviation from the reference reaction path information as did the original ReaxFF and ReaxFF-lg models. Models 5 and 7, the “best” performers identified within this study for overall structural predictions, had rms deviations from the reference reaction path information of 78.1 and 74.7 kcal/mol, respectively. Model 8, the second worst performer had the largest rms deviation from the reference data (94.8 kcal/mol).

4. CONCLUSIONS

A variety of force fields were parametrized to the ReaxFF and ReaxFF-lg forms [eqs 1 and 2, respectively] using the Multiple Objective Evolutionary Strategies (MOES) algorithm, where different numbers of objectives and parameters were allowed to vary. Our goal was to determine if the MOES algorithm could generate a force field that would produce ambient state crystallographic structural results for RDX that were as good as or better than the original ReaxFF and ReaxFF-lg models that were parametrized using nongenetic algorithms and required significant user interaction. Of the numerous Pareto-efficient force fields generated in the MOES search, the various force fields evaluated in this study were chosen based on the ability to predict the RDX ambient crystal lattice parameters. Of these,

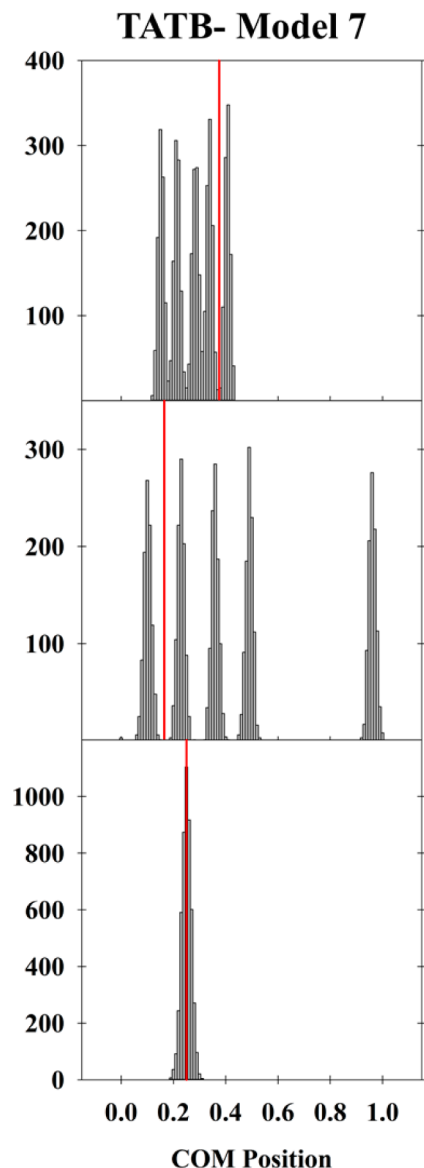


Figure 7. Cumulative distributions of the center of mass fractional coordinates for one of the two symmetry equivalent molecules in the unit cell of TATB for Model 7. Top, middle, and lower frames are the distributions for the x -, y -, and z -fractional positions, respectively. Red vertical line in each frame denotes the experimental position.

Models 4 and 5 had the best overall ability to predict the ambient state crystallographic and molecular structural parameters of RDX and were better than the original ReaxFF and ReaxFF-*lg* force fields. Both models assumed the form of eq 2, with Model 4 allowing only the terms controlling the EEM and van der Waals interactions to vary, while Model 5 allowed the EEM, van der Waals, and the *lg*-parameters to vary. These models used only five objectives in the MOES search, with one objective composed of SAPT(DFT) energies for a large number of dimer configurations of both the RDX and FOX-7 systems. These models had better performances than the models selected from six-objective optimizations, in which the SAPT(DFT) energies for RDX and FOX-7 were partitioned in separate objectives. The Model 7 and ReaxFF-*lg* force fields were the next best performers in predicting the crystallographic and molecular structural parameters of RDX at the ambient state.

The various force fields were used in MD simulations of five other well-known energetic molecular crystals to determine the degree of transferability. In almost all cases, the models that did not include the *-lg* term performed poorly. Performance of the models across the systems was mixed. All but two models provide a good description of the crystal structure of the branched nitroalkane explosive PETN; however, one of these models produced molecular structures that differed significantly from experiment. None of the models well reproduced the crystal structures of FOX-7 or TATB, systems exhibiting extensive hydrogen bonding producing layered structures in which the molecules are fixed in specific orientations and locations within the unit cell. This is notable, since a significant amount of highly accurate QM information for intermolecular interactions of FOX-7 was included in the objectives. For these two systems, most of the models showed that during molecular dynamics simulations, the molecules would undergo significant in-plane translation within the layers, with little motion in the direction perpendicular to the plane of the layers. Also, the majority of the models for FOX-7 showed significant orientational deviations of the molecules within the unit cell, with all but three unable to reproduce the characteristic herringbone lattice structure of the FOX-7 system. Interestingly, the force field in which the hydrogen bonding terms were adjusted in the MOES search (Model 8) did not predict good crystal structures for either FOX-7 or TATB. Instead, this force field predicted molecular structures that differed significantly from experiment, and produced structures that indicated intramolecular hydrogen atom migration had occurred during the trajectory integration. However, the selection of this force field from the Pareto-efficient solutions for Model 8 was based on its ability to predict the RDX crystal structure, not a hydrogen-bonded system, such as FOX-7 or TATB. The RDX crystal does not have a significant amount of hydrogen bonding.

The results clearly indicate that reasonable force fields for energetic molecular crystals can be obtained that have a degree of transferability. However, they are dependent on the training set and the criteria used to select the most promising force field. Additionally, the initial selection using a simple single criterion (i.e., the crystal lattice parameters) does not guarantee that other properties will be equally well described. However, we have demonstrated that the highly complex reactive force field, ReaxFF and its variant, ReaxFF-*lg*, can be parametrized using the MOES process to produce desired results. The benefits of the MOES methodology are that it requires little user intervention and only a rudimentary understanding of the interdependence of the parameters on one another and can generate hundreds to thousands of candidate Pareto-efficient force fields, as compared to a standard single objective style search, which generates a sole candidate force field. While the typical optimization strategies could potentially discover the optimal parameter set in the desired phase space, the probability of any single search doing so is very small. MOES allows for a much more efficient search of phase space and generates multiple, equally optimal parameter sets, making the discovery of an ideal force field much more probable. Additionally, MOES is not restricted to fitting ReaxFF and ReaxFF-*lg* force fields but rather can be used to parametrize any function. It is for these reasons that the MOES methodology and code is well-suited for force field development.

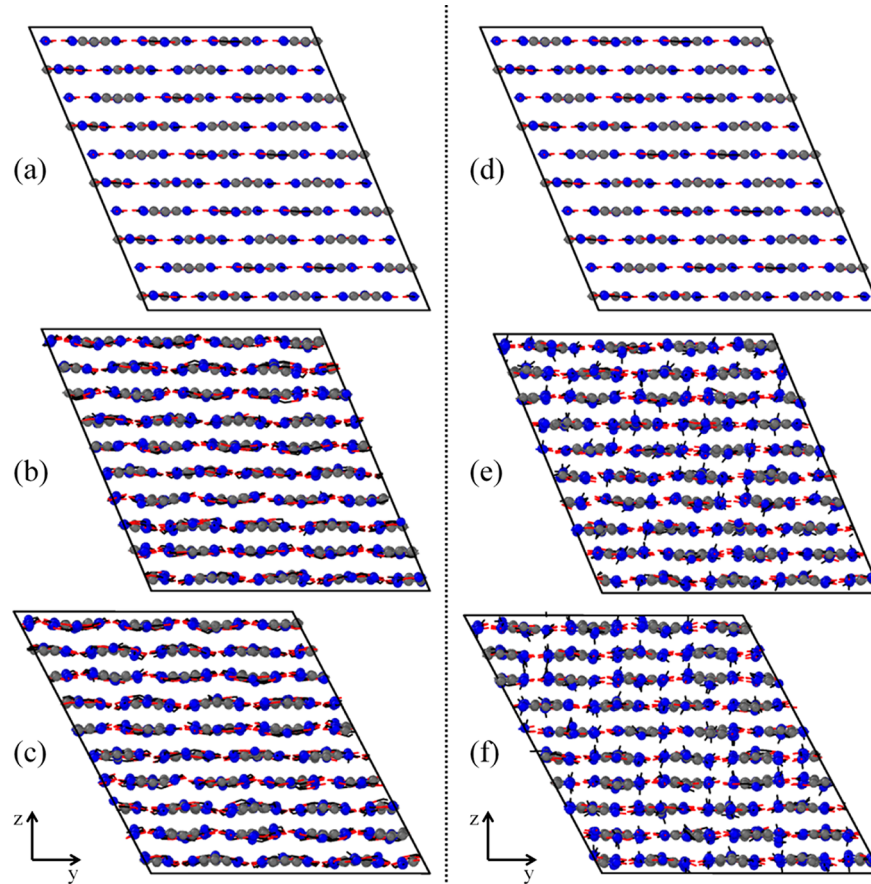


Figure 8. Atomic configurations from simulations of TATB using (a–c) ReaxFF-*lg* and (d–f) Model 7, at the same times described in Figure 5

Table 9. Ranks of Models by Lowest Error for TATB

model	edge lengths ^a	cell angles ^b	COM fractionals ^b	molecular structure ^c	orientation ^c	overall rank
1	9	1	8	9	8	35
2	10	9	1	10	10	40
3	1	8	3	4	5	21
4	8	3	6	7	1	25
5	3	10	4	1	3	21
6	6	7	9	5	4	31
7	4	6	7	8	7	32
8	7	2	10	6	9	34
ReaxFF	5	5	5	3	6	24
ReaxFF- <i>lg</i>	2	4	2	2	2	12

^aAverage absolute percent errors. ^bAverage absolute errors. ^cAverage rms errors.

Table 10. Ranks of the Models by System

model	RDX	HMX	CL20	PETN	FOX-7	TATB	overall rank
5	1	2.5	6	2	9	2.5	23.0
7	3	6	2	5	1	7	24.0
ReaxFF- <i>lg</i>	4	1	7	3	8	1	24.0
4	2	4	3	8	3	5	25.0
6	5	2.5	8	1	4	6	26.5
3	8	5	9	6	5.5	2.5	36.0
ReaxFF	7	8	10	7	2	4	38.0
1	9	7	1	4	10	9	40.0
8	6	9	4	9	7	8	43.0
2	10	10	5	10	5.5	10	50.5

ASSOCIATED CONTENT

Supporting Information

Crystallographic and molecular structural parameters for RDX, HMX, CL-20, PETN, FOX-7, and TATB (Tables S1–S6). Atomistic animations of the equilibration of FOX-7 and TATB with ReaxFF-*lg* and Model 7 (Movies M1–M4). Comparison of rms deviation of all model predictions of the reaction pathway and bond dissociation energies from reference data (Figure S1). This material is available free of charge via the Internet at <http://pubs.acs.org>

AUTHOR INFORMATION

Corresponding Author

*E-mail: neil.s.weingarten.civ@mail.mil. Phone: (410) 306-0718.

Notes

The authors declare no competing financial interest.

ACKNOWLEDGMENTS

This research was supported by the Department of Defense (DOD) High Performance Computing Modernization Program (HCPMP) Software Application Institute for Multiscale Reactive Modeling of Insensitive Munitions and a DOD HPCMP Challenge award. All calculations were performed on the DOD Supercomputer Resource Centers at ARL, ERDC, AFRL, and MHPCC.

REFERENCES

- (1) van Duin, A. C. T.; Dasgupta, S.; Lorant, F.; Goddard, W. A. *J. Phys. Chem. A* **2001**, *105*, 9396.
- (2) Nomura, K.; Kalia, R. K.; Nakano, A.; Vashishta, P.; van Duin, A. C. T.; Goddard, W. A. *Phys. Rev. Lett.* **2007**, *99*, 148303.
- (3) Budzien, J.; Thompson, A. P.; Zybin, S. V. *J. Phys. Chem. B* **2009**, *113*, 13142.
- (4) Zhang, L.; Zybin, S. V.; van Duin, A. C. T.; Dasgupta, S.; Goddard, W. A.; Kober, E. M. *J. Phys. Chem. A* **2009**, *113*, 10619.
- (5) Guo, F.; Zhang, H.; Cheng, X. *J. Theor. Comput. Chem.* **2010**, *9*, 315.
- (6) van Duin, A. C. T.; Zeiri, Y.; Dubnikova, F.; Kosloff, R.; Goddard, W. A. *J. Am. Chem. Soc.* **2005**, *127*, 11053.
- (7) Mortier, W. J.; Ghosh, S. K.; Shankar, S. *J. Am. Chem. Soc.* **1986**, *108*, 4315.
- (8) Liu, L.; Liu, Y.; Zybin, S. V.; Sun, H.; Goddard, W. A. *J. Phys. Chem. A* **2011**, *115*, 11016.
- (9) Larentzos, J. P.; Rice, B. M.; Byrd, E. F. C.; Weingarten, N. S.; Lill, J. *J. Chem. Theory Comput.* **2014**, DOI: 10.1021/ct500788c.
- (10) Williams, H. L.; Chabalowski, C. F. *J. Phys. Chem. A* **2001**, *105*, 646.
- (11) Podeszwa, R.; Bukowski, R.; Rice, B. M.; Szalewicz, K. *Phys. Chem. Chem. Phys.* **2011**, *13*, 16629.
- (12) Taylor, D. E.; Rob, F.; Rice, B. M.; Podeszwa, R.; Szalewicz, K. *Phys. Chem. Chem. Phys.* **2007**, *9*, 5561.
- (13) Lill, J. V.; Yau, A. *Multiple Objective Evolution Strategies (MOES): A User's Guide to Running the Software*; ARL-CR-0753, Army Research Laboratory: Aberdeen Proving Ground, MD, US, **2014**.
- (14) Plimpton, S. *J. Comput. Phys.* **1995**, *117*, 1.
- (15) Allen, F. H. *Acta Crystallogr.* **2002**, *B58*, 380.
- (16) Choi, C. S.; Prince, E. *Acta Crystallogr., Sect. B: Struct. Crystallogr. Cryst. Chem.* **1972**, *28*, 2857.
- (17) Choi, C. S.; Boutin, H. P. *Acta Crystallogr., Sect. B: Struct. Crystallogr. Cryst. Chem.* **1970**, *26*, 1235.
- (18) Nielsen, A. T.; Chafin, A. P.; Christian, S. L.; Moore, D. W.; Nadler, M. P.; Nissan, R. A.; Vanderah, D. J.; Gilardi, R.; George, C. F.; Flippin-Anderson, J. L. *Tetrahedron* **1998**, *54*, 11793.
- (19) Zhurova, E. A.; Stash, A. I.; Tsirelson, V. G.; Zhurov, V. V.; Bartashevich, E. V.; Potemkin, V. A.; Pinkerton, A. A. *J. Am. Chem. Soc.* **2006**, *129*, 14728.
- (20) Gilardi, R. Naval Research Laboratory, 1999 Private Communication; Deposition CCDC 127539.
- (21) Cady, H. H.; Larson, A. C. *Acta Crystallogr.* **1965**, *18*, 485.
- (22) Kearsley, S. K. *Acta Crystallogr. A* **1989**, *45*, 208.
- (23) Aguirre, O.; Taboada, H.; Coit, D.; Wattanapongsakorn, N. *Proceedings of the 2011 IEEE ICQR*; IEEE: New York, 2011; pp 225–229.
- (24) Carillo, V. M.; Taboada, H. *Procedia Comput. Sci.* **2012**, *12*, 116.
- (25) Carrillo, V. M.; Aguirre, O.; Taboada, H. *Procedia Comput. Sci.* **2011**, *6*, 243.
- (26) Li, Z.; Liao, H.; Coit, D. W. *Reliab. Eng. Syst. Safety* **2009**, *94*, 1585.
- (27) Aguirre, O.; Taboada, H. *Procedia Comput. Sci.* **2011**, *6*, 195.